Towards Timetronics with Photonic Systems

Ali Emami Kopaei,[1,2,*] Karthik Subramaniam Eswaran,[1,2] Arkadiusz Kosior,[3] Daniel Hodgson,[4] Andrey Matsko,[5] Hossein Taheri,[6] Almut Beige,[4] and Krzysztof Sacha[2,7,†]

[1] *Szkoła Doktorska Nauk Ścisłych i Przyrodniczych, Wydział Fizyki, Astronomii i Informatyki Stosowanej, Uniwersytet Jagielloński, ulica Profesora Stanisława Łojasiewicza 11, PL-30-348 Kraków, Poland*

[2] *Instytut Fizyki Teoretycznej, Wydział Fizyki, Astronomii i Informatyki Stosowanej, Uniwersytet Jagielloński, ulica Profesora Stanisława Łojasiewicza 11, PL-30-348 Kraków, Poland*

[3] *Institut für Theoretische Physik, Universität Innsbruck, A-6020 Innsbruck, Austria*

[4] *School of Physics and Astronomy, University of Leeds, Leeds, UK, LS2 9JT*

[5] *Jet Propulsion Laboratory, California Institute of Technology, 4800 Oak Grove Drive, Pasadena, California 91109-8099, USA*

[6] *Department of Electrical and Computer Engineering, University of California Riverside, 3401 Watkins Drive, Riverside, CA 92521*

[7] *Centrum Marka Kaca, Uniwersytet Jagielloński, ulica Profesora Stanisława Łojasiewicza 11, PL-30-348 Kraków, Poland*

(Dated: September 13, 2024)

Periodic driving of systems of particles can create crystalline structures in time. Such systems can be used to study solid-state physics phenomena in the time domain. In addition, it is possible to engineer the wave-number band structure of optical systems and to realize photonic time crystals by periodic temporal modulation of the material properties of the electromagnetic wave propagation medium. We introduce here a versatile averaged-permittivity approach which empowers emulating various condensed matter phases in the time dimension in a traveling wave resonator. This is achieved by utilizing temporal modulation of permittivity within a small segment of the resonator and the spatial shape of the segment. The required frequency and depth of the modulation are experimentally achievable, opening a pathway for research into the practical realisation of crystalline structures in time utilising microwave and optical systems.

Electromagnetic waves can propagate in media where the refractive index changes periodically in space or time [1–3]. In the first case, we have photonic crystals in space, which exhibit a band structure in the frequency domain. In the second case, we deal with photonic time crystals, where the wave number domain reveals a band structure. In the optical regime, the experimental realization of photonic time crystals is a formidable challenge because the required modulation depth of the refractive index must be significant, and the frequency of its changes comparable to optical frequencies [4].

In periodically driven atomic and solid-state systems, as well as in nonlinear optical systems, it is possible to realize discrete time crystals that spontaneously break discrete translational symmetry in time and begin to evolve with a period longer than that dictated by the periodic perturbation [5–27]. New periodic evolution forms spontaneously, creating new crystalline structures in time. Periodically perturbed atomic systems are also well-suited for realizing a wide range of phases known from condensed matter physics, but observed in the time dimension [28–30], such as Anderson and many-body localization [31, 32], Mott and topological insulators [33, 34], fractonic excitations [35], as well as higher-dimensional topological systems [36, 37]. The flexibility of controlling and modifying various solid-state physics behaviors in time through periodic perturbation control suggests practical applications. Analogous to electronics, timetronics concerns the research and design of potentially useful devices where crystalline structures in time play a key role [38].

In this Letter, we pave the way for *optical timetronics* by demonstrating that a simple traveling wave resonator can exhibit a broad range of condensed matter phases or combinations of different phases, observed in the time domain. For example, phases like Anderson or topological insulators can be realized, different behaviors can be connected together, external fields can be realized and can act during a certain phase or the entire experiment, and the whole system can be completely reconfigured at any moment during the experiment. All of this is possible through time periodic modulation of the permittivity adapted to the shape of the small fragment of the resonator where the modulation is performed. That is, temporal harmonics of the modulation match resonantly with spatial harmonics of the resonator fragment and determine the effective behavior of the system. The described time modulation is experimentally feasible and allows for processing electromagnetic signals using phenomena known in condensed matter physics, thus paving the way for timetronics, i.e., applications where crystalline structures in time play a crucial role [38]. We present our idea by providing a detailed prescription for designing an arbitrary one-dimensional band structure. We then present two specific examples: the Su–Schrieffer–Heeger (SSH) model [39, 40] and the Wannier-Stark ladder [41, 42].

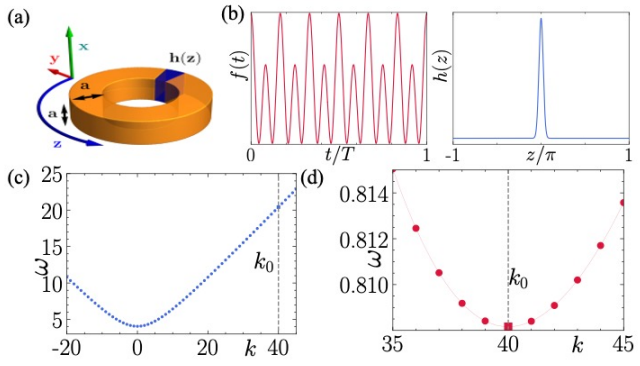

FIG. 1. (a) Resonator in the form of a closed ring with a square cross-section. The circumference of the ring, in the units used in the text, is 2π. In a small segment of the resonator described by $h(z)$, the permittivity is periodically modulated in time with the frequency $\Omega = 2\pi/T$. (b) Example of the periodic modulation, $f(t)$, of the permittivity (left) in a small fragment of the resonator described by $h(z)$ of the Gaussian shape (right). This example is analyzed in the text. (c) Dispersion relation (in the laboratory frame) for longitudinal modes of the resonator with the length of the side of the cross-section area of the resonator $a = 0.54$. Points indicate the discrete spectrum of the ring-shaped resonator. (d) In the frame moving with the frequency Ω which matches the free spectral range of the resonator, the dispersion relation for the longitudinal modes has a minimum at $k_0 = 40$, and superpositions of waves with $k \approx k_0$ evolve extremely slowly.

As an illustration of our idea, let us consider a closed resonator in the form of a ring with a square cross-section [Fig. 1(a)]. For simplicity, we re-scale the magnetic field vector, $\mathbf{H} \to \sqrt{\varepsilon_0/\mu_0}\,\mathbf{H}$, and use $L/2\pi$ and $L/2\pi c$ as the units of length and time, respectively, where L is the circumference of the ring, c is the speed of light, and μ_0 and ε_0 are the vacuum permeability and permittivity [43]. Most importantly, we assume that the relative permittivity of a material ε is constant everywhere in the resonator except for a small segment where ε changes periodically in time according to

$$\varepsilon(z,t) = \varepsilon_r + h(z)f(t) \quad \text{with} \quad f(t+T) = f(t), \qquad (1)$$

for example, as in Fig. 1(b). Here z denotes the position along the resonator and $h(z)$ and $f(t)$ are functions which vary in space and time respectively and describe the small segment of the resonator. In numerical calculations we set $\varepsilon_r = 4$.

Next, we assume that the TE_{11} mode of the electromagnetic field has been injected into the resonator [43]. In this case, the electric field does not have a longitudinal component and we only need to consider the dependence of the transverse electric field amplitude $E(z,t)$ on time and space. Since $\varepsilon(z,t)$ is a periodic function of time, we can apply the Floquet theorem [28, 44] and seek solutions of Maxwell equations in the form $E(z,t) = \widetilde{E}(z,t)e^{i\omega t}$ with $\widetilde{E}(z,t+T) = \widetilde{E}(z,t)$. Here ω denotes the quasi-frequency of the electromagnetic field. The general solution of Maxwell equations can be obtained as a superposition of solutions $\widetilde{E}(z,t)e^{i\omega t}$. When solving Maxwell equations, it is convenient not to fully eliminate the magnetic field and to reduce them instead to a generalized eigenvalue problem

$$\begin{bmatrix} -i\partial_t\varepsilon - i\varepsilon\partial_t & \frac{i}{2k_\perp}\partial_z^2 - ik_\perp \\ 2ik_\perp & -i\partial_t \end{bmatrix} \begin{bmatrix} \widetilde{E} \\ \widetilde{H} \end{bmatrix} = \omega \begin{bmatrix} \varepsilon & 0 \\ 0 & 1 \end{bmatrix} \begin{bmatrix} \widetilde{E} \\ \widetilde{H} \end{bmatrix} \qquad (2)$$

with eigenvalue ω [43]. In this equation, $H(z,t) = \widetilde{H}(z,t)e^{i\omega t}$, with $\widetilde{H}(z,t+T) = \widetilde{H}(z,t)$, is the amplitude of the longitudinal component of the magnetic field and $k_\perp = \pi/a$ with a being the normalized length of each side of the cross-sectional area of the resonator [Fig. 1(a)].

If there is no modulation in time of the permittivity (i.e., if $f(t) = 0$), the solutions of Maxwell equations are characterized by a nonlinear dispersion relation $\omega = \sqrt{2k_\perp^2 + k^2}$ where the wave number k of the longitudinal modes takes integer values because we are considering the resonator in the form of a closed ring with periodic boundary conditions (Fig. 1). Let us assume that the permittivity is periodically modulated in time with the frequency $\Omega = 2\pi/T$ and that the resonance condition with the frequency of a wave packet circulation around the resonator is satisfied, i.e., Ω matches the free spectral range of the resonator. In other words there exists a wave number k_0 for which the group velocity (calculated in the absence of the modulation) $\partial\omega/\partial k|_{k=k_0} = \Omega$ where the new units have been applied. For the sufficiently long resonator, the frequency Ω of the permittivity modulation is within the experimentally achievable range, e.g., for $L = 1$ cm, $\Omega = 15$ GHz.

To simplify the description of the resonant behavior of the system, we will switch to a reference frame evolving with the modulation frequency $z' = z - \Omega t$ using the transformation $U = e^{\Omega t\partial_z}$ [43]. In the moving frame, the dispersion relation has a quadratic behavior with the minimum at the resonant wave number k_0, i.e. $\omega \approx \omega(k_0) + \partial^2\omega/\partial k^2|_{k=k_0}(k-k_0)^2/2$, see Fig. 1(d). In the present work we assume that the group velocity dispersion results from the geometry of the resonator but in general there can also be a contribution from the material properties of the resonator. In the moving frame, the evolution of a superposition of waves with wave numbers $k \approx k_0$ proceeds very slowly, and we can average Maxwell equations over time. This is essentially the rotating wave approximation, leading to time-independent effective Maxwell equations in the moving frame [28, 43, 45]:

$$\begin{bmatrix} i\Omega\partial_z\bar{\varepsilon} + i\Omega\bar{\varepsilon}\partial_z & \frac{i}{2k_\perp}\partial_z^2 - ik_\perp \\ 2ik_\perp & i\Omega\partial_z \end{bmatrix} \begin{bmatrix} \widetilde{E} \\ \widetilde{H} \end{bmatrix} = \omega \begin{bmatrix} \bar{\varepsilon} & 0 \\ 0 & 1 \end{bmatrix} \begin{bmatrix} \widetilde{E} \\ \widetilde{H} \end{bmatrix}. \qquad (3)$$

For clarity, we omitted the primes indicating that all variables and quantities refer to the moving frame. Moreover,

the time-averaged permittivity $\bar{\varepsilon}(z)$ in the above equation can be written as

$$\bar{\varepsilon}(z) = \varepsilon_r + \frac{1}{T}\int_0^T \mathrm{d}t\; h(z+\Omega t) f(t) = \varepsilon_r + \sum_m h_m f_{-m} e^{imz}, \tag{4}$$

after introducing the Fourier expansions $h(z) = \sum_m h_m e^{imz}$ and $f(t) = \sum_l f_l e^{il\Omega t}$.

In the moving frame, the effective Maxwell equations (3) describe electromagnetic waves in a resonator with a time-averaged permittivity $\bar{\varepsilon}(z)$ which varies in space along the resonator. In the laboratory frame, the segment of the resonator in which the permittivity is modulated in time is described by a localized function $h(z)$ and, therefore, has many non-zero Fourier coefficients h_m. The Fourier expansion coefficients of $f(t)$ can be chosen to realize any average permittivity $\bar{\varepsilon}(z)$ in the effective description in the moving frame since $\bar{\varepsilon}(z)$ can always be expanded such that $\bar{\varepsilon}(z) = \varepsilon_r + \sum_m \varepsilon_m e^{imz}$. All we need to do to obtain the given $\bar{\varepsilon}(z)$ in (4) is to choose $f(t)$ such that its Fourier coefficients satisfy $f_{-m} = \varepsilon_m/h_m$. For example, we can realize $\bar{\varepsilon}(z) \propto \cos(sz)$ with integer $s \gg 1$ and observe a band structure in the quasi-frequency, ω, domain. We can realize a topological insulator or introduce disorder in a crystalline structure and realize a Anderson insulator. We can also combine crystalline structures with different properties, e.g., in different regions of z, the average permittivity $\bar{\varepsilon}(z)$ can reveal topologically different structures. Static electric field like potential, barriers or wells or more complex behavior can be realized in $\bar{\varepsilon}(z)$. Note that a stationary solution of (3) will appear as a propagating solution when we return to the laboratory frame. Thus, any condensed matter like behavior which we realize and observe versus z in the moving frame will be observed in the time domain if, in the laboratory frame, we place a detector at a certain position z_0 in the resonator and investigate its clicking in time. This paves the way for optical timetronics, i.e., similar to electronics, we can design time-varying optical systems where electromagnetic signals are processed employing phenomena known in solid-state physics [38].

As a first example, we consider a system that can reveal topologically protected edge states in the time domain [28, 30, 47–50]. Suppose $k_\perp = 5.74$, $h(z) = e^{-z^2/2\sigma^2}$ with $\sigma = \pi/41$ and $f(t) = (\lambda_1/h_{s/2})\cos(s\Omega t/2) + (\lambda_2/h_s)\cos(s\Omega t)$ with s being even, with $\Omega = 0.49$ and with $h_{s/2}$ and h_s denoting the Fourier coefficients of $h(z)$, see Fig. 1(b). In the moving frame, the resulting average permittivity takes the form of a crystalline structure in space with a two-point basis,

$$\bar{\varepsilon}(z) = \varepsilon_r + \lambda_1 \cos(sz/2) + \lambda_2 \cos(sz). \tag{5}$$

The quasi-frequency spectra obtained for $s = 12$ with the help of the effective approach (3) and by solving the Maxwell equations (2) exactly are presented in Fig. 2(a).

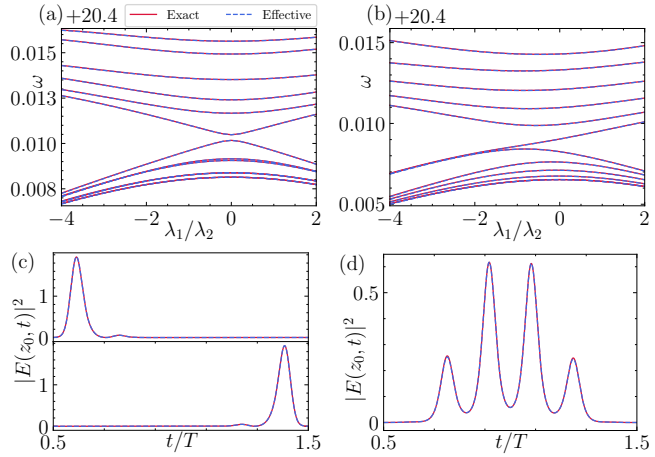

FIG. 2. (a) Quasi-frequency spectra corresponding to the exact and effective Maxwell equations. In the effective equations, the averaged permittivity is described by (5), where $s = 12$ and $\lambda_2 = 2\pi \times 10^{-3}$. (b) The same as in (a), but in the presence of additional time modulation of the permittivity, which leads to a Gaussian barrier in (5) with a width of $\sqrt{2}\pi/41$ and $\lambda_b = -4.3 \times 10^{-2}$ located at $z = 0$. For $\lambda_1 < 0$, the formation of degenerate levels in the gap of the quasi-frequency bands can be observed. (c) Variations of the electric field at position $z_0 = \pi$ in the laboratory frame corresponding to two quasi-frequency levels located in the gap between two bands in (b) for $\lambda_1/\lambda_2 = -4$. The field is localized around the moment in time when a Gaussian barrier in $\bar{\varepsilon}(z_0 - \Omega t)$ appears at the position z_0 [46]. (d) Similar to (c) but for a state from one of the bands. Such bulk states are delocalized along the entire period T. In all panels, both the exact results and the results of the effective Maxwell equations are presented.

Both solutions match each other very well. For example, for $\lambda_1 = 0$, we observe a single band in the quasi-frequency domain consisting of $s = 12$ levels. When λ_1 starts to differ from zero, the crystalline structure in $\bar{\varepsilon}(z)$ has a two-point basis and the initially single band splits into two. When we focus on these two bands, the band structure of the system is equivalent to the well-known SSH model which reveals topologically protected edge states in the presence of edges and in the topologically nontrivial regime [39, 40]. The crystalline structure in (5) is a periodic structure in a resonator without any edge. However, by a proper additional time modulation of the permittivity we can introduce a localized barrier in the crystalline structure and thus an edge in the system. Indeed, by introducing an additional modulation to our chosen $f(t)$ in the form of $\lambda_b\, e^{-t^2\Omega^2/2\sigma^2}$ we create a barrier in $\bar{\varepsilon}(z)$ represented by a Gaussian function with a width of $\sqrt{2}\pi/41$. In this case, we observe the appearance of two levels in the quasi-frequency spectrum located in the gap if $\lambda_1 < 0$ [Fig. 2(b)]. In the moving frame, the electromagnetic fields corresponding to these levels are localized on either side of the barrier, i.e. they are topologically protected edge states [40]. In the labo-

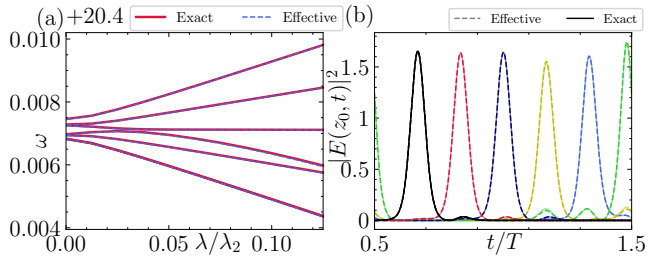

FIG. 3. (a) Quasi-frequency spectrum as a function of the strength, λ, of the artificial static electric field generated in (5) by the additional time modulation of the permittivity (see text) for $s = 6$, $\lambda_1 = 0$ and $\lambda_2 = 4 \times 10^{-3}$. (b) In the presence of the artificial static electric field, five solutions of the Maxwell equations exhibit Stark localization which in the laboratory frame we observe in the time domain. Namely, the electromagnetic fields at a fixed position in the laboratory frame (here $z_0 = \pi$) are localized at different moments in time. These moments correspond to different local minima of $\bar{\varepsilon}(z_0 - \Omega t)$. There is one more solution (green curve) localized around the discontinuity in $\bar{\varepsilon}(z_0 - \Omega t)$ corresponding to the third quasi-frequency level in (a). The presented states correspond to $\lambda/\lambda_2 = 0.125$.

ratory frame, if we place a detector at a certain position z_0 in the resonator, we can observe these edge states in the time domain [28, 30, 47–49]. This means, temporal changes of the probability of the detector clicking reveal the appearance of an edge state in time when the edge in $\bar{\varepsilon}(z_0 - \Omega t)$ reaches the detector position. In Figs. 2(c)-2(d), we present how the electric field changes in time at the detector position for both the edge states and the so-called bulk states. The latter are delocalized in time across the entire period $T = 2\pi/\Omega$. Note that the modulation depth of the permittivity needed to realize the described phenomena is very small, i.e. maximally of the order 10^{-2}.

As a second example, we consider the introduction of an artificial static electric field in the crystalline structure described by (5) and predict the observation of the Wannier-Stark localization in the optical system [41, 42]. Knowing the Fourier expansion of the linear potential in a resonator, $\lambda(z - \pi) = i\lambda \sum_{m\neq 0} e^{imz}/m$, we can introduce additional Fourier coefficients in $f(t)$, i.e. $f_{-m} = i\lambda/(mh_m)$, which lead to a tilted crystalline structure and thus the presence of an artificial static electric field in our system. Note that in a ring-shaped resonator, the linear potential has a discontinuity at $z = 0$ (or equivalently $z = 2\pi$). However, away from $z = 0$, the influence of the boundary conditions is negligible, and we can observe states that lose the character of extended Bloch waves and localize in different cells of the tilted crystalline structure $\bar{\varepsilon}(z)$. In the case of $s = 6$, which is presented in Fig. 3, we see five such states with equally spaced quasi-frequencies. There is one more state localized around the discontinuity whose quasi-frequency falls between the second and third equally spaced eigenvalues [Fig. 3(a)]. In the laboratory frame, with a detector at a certain position z_0 in the resonator, we can observe the electromagnetic field localized at different moments in time [Fig. 3(b)].

In summary, we demonstrate that the properties of electromagnetic waves propagating in a resonator with a time-modulated refractive index can exhibit a range of behaviors known from research of crystalline structures in space, but observed in the time domain. Furthermore, different time crystalline structures can be combined by choosing the appropriate time modulation. Importantly, the realization of these structures in the optical regime does not require either deep modulation of the refractive index or modulation frequencies comparable to optical frequencies, as is the case in already known photonic time crystals. Thus, we obtain a tool that allows for processing of electromagnetic signals where time crystalline structures play a key role and can have practical applications. This paves the way for optical timetronics. As an example, in this Letter we considered a resonator in the shape of a one-dimensional ring due to the simplicity of their theoretical description. In our analysis, we have quantitatively examined the necessary conditions to realize the Su–Schrieffer–Heeger and Wannier-Stark ladder models, but our findings extend well beyond these particular cases. Notably, the introduction of a non-linear medium, where the permittivity varies with the electric field strength, enables us to introduce interactions. This capability opens up new opportunities to explore and study a wide range of condensed matter phases and phenomena.

The data that support the findings of this study are available from the corresponding author upon reasonable request.

Acknowledgment. This research was funded by the National Science Centre, Poland, Project No. 2021/42/A/ST2/00017. The numerical computations in this work were supported in part by PL-Grid Infrastructure, Project No. PLG/2023/016644. This research was funded in whole or in part by the Austrian Science Fund (FWF) [grant DOI: 10.55776/ESP171]. HT was supported by the National Science Foundation of the United States of America under Grant No. 2131402. Research conducted by AM was carried out at the Jet Propulsion Laboratory, California Institute of Technology, under a contract with the National Aeronautics and Space Administration (80NM0018D0004). DH acknowledges funding from the UK Engineering and Physical Sciences Research Council EPSRC [grant number EP/W524372/1].

* ali.emami.app@gmail.com

† krzysztof.sacha@uj.edu.pl

[1] E. Galiffi, R. Tirole, S. Yin, H. Li, S. Vezzoli, P. A. Huidobro, M. G. Silveirinha, R. Sapienza, A. Alù, and J. B. Pendry, Photonics of time-varying media, Advanced Photonics **4**, 014002 (2022).

[2] J. B. Pendry and S. A. R. Horsley, Qed in space-time varying materials, APL Quantum **1**, 020901 (2024).

[3] S. A. Schulz, R. F. Oulton, M. Kenney, A. Alù, I. Staude, A. Bashiri, Z. Fedorova, R. Kolkowski, A. F. Koenderink, X. Xiao, J. Yang, W. J. Peveler, A. W. Clark, G. Perrakis, A. C. Tasolamprou, M. Kafesaki, A. Zaleska, W. Dickson, D. Richards, A. Zayats, H. Ren, Y. Kivshar, S. Maier, X. Chen, M. A. Ansari, Y. Gan, A. Alexeev, T. F. Krauss, A. Di Falco, S. D. Gennaro, T. Santiago-Cruz, I. Brener, M. V. Chekhova, R.-M. Ma, V. V. Vogler-Neuling, H. C. Weigand, Ü.-L. Talts, I. Occhiodori, R. Grange, M. Rahmani, L. Xu, S. M. Kamali, E. Arababi, A. Faraon, A. C. Harwood, S. Vezzoli, R. Sapienza, P. Lalanne, A. Dmitriev, C. Rockstuhl, A. Sprafke, K. Vynck, J. Upham, M. Z. Alam, I. De Leon, R. W. Boyd, W. J. Padilla, J. M. Malof, A. Jana, Z. Yang, R. Colom, Q. Song, P. Genevet, K. Achouri, A. B. Evlyukhin, U. Lemmer, and I. Fernandez-Corbaton, Roadmap on photonic metasurfaces, Applied Physics Letters **124**, 260701 (2024).

[4] E. Lustig, O. Segal, S. Saha, C. Fruhling, V. M. Shalaev, A. Boltasseva, and M. Segev, Photonic time-crystals - fundamental concepts [invited], Opt. Express **31**, 9165 (2023).

[5] K. Sacha, Modeling spontaneous breaking of time-translation symmetry, Phys. Rev. A **91**, 033617 (2015).

[6] V. Khemani, A. Lazarides, R. Moessner, and S. L. Sondhi, Phase structure of driven quantum systems, Phys. Rev. Lett. **116**, 250401 (2016).

[7] D. V. Else, B. Bauer, and C. Nayak, Floquet time crystals, Phys. Rev. Lett. **117**, 090402 (2016).

[8] J. Zhang, P. W. Hess, A. Kyprianidis, P. Becker, A. Lee, J. Smith, G. Pagano, I.-D. Potirniche, A. C. Potter, A. Vishwanath, N. Y. Yao, and C. Monroe, Observation of a discrete time crystal, Nature **543**, 217 (2017).

[9] S. Choi, J. Choi, R. Landig, G. Kucsko, H. Zhou, J. Isoya, F. Jelezko, S. Onoda, H. Sumiya, V. Khemani, C. von Keyserlingk, N. Y. Yao, E. Demler, and M. D. Lukin, Observation of discrete time-crystalline order in a disordered dipolar many-body system, Nature **543**, 221 (2017).

[10] S. Pal, N. Nishad, T. S. Mahesh, and G. J. Sreejith, Temporal order in periodically driven spins in star-shaped clusters, Phys. Rev. Lett. **120**, 180602 (2018).

[11] J. Rovny, R. L. Blum, and S. E. Barrett, Observation of discrete-time-crystal signatures in an ordered dipolar many-body system, Phys. Rev. Lett. **120**, 180603 (2018).

[12] J. Smits, L. Liao, H. T. C. Stoof, and P. van der Straten, Observation of a space-time crystal in a superfluid quantum gas, Phys. Rev. Lett. **121**, 185301 (2018).

[13] X. Mi, M. Ippoliti, C. Quintana, A. Greene, Z. Chen, J. Gross, F. Arute, K. Arya, J. Atalaya, R. Babbush, J. C. Bardin, J. Basso, A. Bengtsson, A. Bilmes, A. Bourassa, L. Brill, M. Broughton, B. B. Buckley, D. A. Buell, B. Burkett, N. Bushnell, B. Chiaro, R. Collins, W. Courtney, D. Debroy, S. Demura, A. R. Derk, A. Dunsworth, D. Eppens, C. Erickson, E. Farhi, A. G. Fowler, B. Foxen, C. Gidney, M. Giustina, M. P. Harrigan, S. D. Harrington, J. Hilton, A. Ho, S. Hong, T. Huang, A. Huff, W. J. Huggins, L. B. Ioffe, S. V. Isakov, J. Iveland, E. Jeffrey, Z. Jiang, C. Jones, D. Kafri, T. Khattar, S. Kim, A. Kitaev, P. V. Klimov, A. N. Korotkov, F. Kostritsa, D. Landhuis, P. Laptev, J. Lee, K. Lee, A. Locharla, E. Lucero, O. Martin, J. R. McClean, T. McCourt, M. McEwen, K. C. Miao, M. Mohseni, S. Montazeri, W. Mruczkiewicz, O. Naaman, M. Neeley, C. Neill, M. Newman, M. Y. Niu, T. E. O'Brien, A. Opremcak, E. Ostby, B. Pato, A. Petukhov, N. C. Rubin, D. Sank, K. J. Satzinger, V. Shvarts, Y. Su, D. Strain, M. Szalay, M. D. Trevithick, B. Villalonga, T. White, Z. J. Yao, P. Yeh, J. Yoo, A. Zalcman, H. Neven, S. Boixo, V. Smelyanskiy, A. Megrant, J. Kelly, Y. Chen, S. L. Sondhi, R. Moessner, K. Kechedzhi, V. Khemani, and P. Roushan, Time-crystalline eigenstate order on a quantum processor, Nature **601**, 531 (2022).

[14] J. Randall, C. E. Bradley, F. V. van der Gronden, A. Galicia, M. H. Abobeih, M. Markham, D. J. Twitchen, F. Machado, N. Y. Yao, and T. H. Taminiau, Many-body–localized discrete time crystal with a programmable spin-based quantum simulator, Science **374**, 1474 (2021), arXiv:2107.00736 [quant-ph].

[15] P. Frey and S. Rachel, Realization of a discrete time crystal on 57 qubits of a quantum computer, Science Advances **8**, eabm7652 (2022), https://www.science.org/doi/pdf/10.1126/sciadv.abm7652.

[16] H. Keßler, P. Kongkhambut, C. Georges, L. Mathey, J. G. Cosme, and A. Hemmerich, Observation of a dissipative time crystal, Phys. Rev. Lett. **127**, 043602 (2021).

[17] A. Kyprianidis, F. Machado, W. Morong, P. Becker, K. S. Collins, D. V. Else, L. Feng, P. W. Hess, C. Nayak, G. Pagano, N. Y. Yao, and C. Monroe, Observation of a prethermal discrete time crystal, Science **372**, 1192 (2021), https://www.science.org/doi/pdf/10.1126/science.abg8102.

[18] H. Xu, J. Zhang, J. Han, Z. Li, G. Xue, W. Liu, Y. Jin, and H. Yu, Realizing discrete time crystal in an one-dimensional superconducting qubit chain (2021), arXiv:2108.00942 [quant-ph].

[19] H. Taheri, A. B. Matsko, L. Maleki, and K. Sacha, All-optical dissipative discrete time crystals, Nature Communications **13**, 848 (2022).

[20] H. Taheri, A. B. Matsko, T. Herr, and K. Sacha, Dissipative discrete time crystals in a pump-modulated Kerr microcavity, Communications Physics **5**, 1 (2022).

[21] H. Taheri, AB. Matsko, L. Maleki, and K. Sacha, Time Crystals in Optics, Optics and Photonics News , 9 (July/August 2022).

[22] T. Liu, J.-Y. Ou, K. F. MacDonald, and N. I. Zheludev, Photonic metamaterial analogue of a continuous time crystal, Nature Physics **19**, 986 (2023).

[23] Z. Bao, S. Xu, Z. Song, K. Wang, L. Xiang, Z. Zhu, J. Chen, F. Jin, X. Zhu, Y. Gao, Y. Wu, C. Zhang, N. Wang, Y. Zou, Z. Tan, A. Zhang, Z. Cui, F. Shen, J. Zhong, T. Li, J. Deng, X. Zhang, H. Dong, P. Zhang, Y.-R. Liu, L. Zhao, J. Hao, H. Li, Z. Wang, C. Song, Q. Guo, B. Huang, and H. Wang, Schrödinger cats growing up to 60 qubits and dancing in a cat scar enforced discrete time crystal, arXiv e-prints , arXiv:2401.08284 (2024), arXiv:2401.08284 [quant-ph].

[24] K. Shinjo, K. Seki, T. Shirakawa, R.-Y. Sun, and S. Yunoki, Unveiling clean two-dimensional discrete time quasicrystals on a digital quantum computer, arXiv e-prints , arXiv:2403.16718 (2024), arXiv:2403.16718 [quant-ph].

[25] B. Liu, L.-H. Zhang, Z.-K. Liu, J. Zhang, Z.-Y. Zhang, S.-Y. Shao, Q. Li, H.-C. Chen, Y. Ma, T.-Y. Han, Q.-F. Wang, D.-S. Ding, and B.-S. Shi, Higher-order and fractional discrete time crystals in Floquet-driven Rydberg atoms, arXiv e-prints , arXiv:2402.13657 (2024), arXiv:2402.13657 [cond-mat.quant-gas].

[26] B. Liu, L.-H. Zhang, Y. Ma, T.-Y. Han, Q.-F. Wang, J. Zhang, Z.-Y. Zhang, S.-Y. Shao, Q. Li, H.-C. Chen, Y.-J. Wang, J.-D. Nan, Y.-M. Yin, D.-S. Ding, and B.-S. Shi, Microwave seeding time crystal in Floquet driven Rydberg atoms, arXiv e-prints , arXiv:2404.12180 (2024), arXiv:2404.12180 [cond-mat.quant-gas].

[27] A. E. Kopaei, K. Sacha, and L. Guo, Classical phase space crystals in an open environment, Phys. Rev. B **107**, 214302 (2023).

[28] K. Sacha, *Time Crystals* (Springer International Publishing, Switzerland, Cham, 2020).

[29] L. Guo, *Phase Space Crystals*, 2053-2563 (IOP Publishing, 2021).

[30] P. Hannaford and K. Sacha, Condensed matter physics in big discrete time crystals, Association of Asia Pacific Physical Societies Bulletin **32**, 12 (2022), arXiv:2202.05544 [cond-mat.quant-gas].

[31] K. Sacha and D. Delande, Anderson localization in the time domain, Phys. Rev. A **94**, 023633 (2016).

[32] M. Mierzejewski, K. Giergiel, and K. Sacha, Many-body localization caused by temporal disorder, Phys. Rev. B **96**, 140201 (2017).

[33] K. Sacha, Anderson localization and Mott insulator phase in the time domain, Sci. Rep. **5**, 10787 (2015).

[34] K. Giergiel, A. Dauphin, M. Lewenstein, J. Zakrzewski, and K. Sacha, Topological time crystals, New Journal of Physics **21**, 052003 (2019).

[35] K. Giergiel, R. Lier, P. Surówka, and A. Kosior, Bose-hubbard realization of fracton defects, Phys. Rev. Res. **4**, 023151 (2022).

[36] K. Giergiel, A. Kuroś, A. Kosior, and K. Sacha, Inseparable time-crystal geometries on the möbius strip, Phys. Rev. Lett. **127**, 263003 (2021).

[37] Y. Braver, E. Anisimovas, and K. Sacha, Eight-dimensional topological systems simulated using time-space crystalline structures, Phys. Rev. B **108**, L020303 (2023).

[38] K. Giergiel, P. Hannaford, and K. Sacha, Time-tronics: from temporal printed circuit board to quantum computer, arXiv e-prints , arXiv:2406.06387 (2024), arXiv:2406.06387 [cond-mat.quant-gas].

[39] W. P. Su, J. R. Schrieffer, and A. J. Heeger, Solitons in polyacetylene, Phys. Rev. Lett. **42**, 1698 (1979).

[40] J. Asbóth, L. Oroszlány, and A. Pályi, *A Short Course on Topological Insulators: Band Structure and Edge States in One and Two Dimensions*, Lecture Notes in Physics (Springer International Publishing, 2016).

[41] G. H. Wannier, Dynamics of band electrons in electric and magnetic fields, Rev. Mod. Phys. **34**, 645 (1962).

[42] P. M. Preiss, R. Ma, M. E. Tai, A. Lukin, M. Rispoli, P. Zupancic, Y. Lahini, R. Islam, and M. Greiner, Strongly correlated quantum walks in optical lattices, Science **347**, 1229 (2015), https://www.science.org/doi/pdf/10.1126/science.1260364.

[43] See Supplemental Material.

[44] J. H. Shirley, Solution of the schrödinger equation with a hamiltonian periodic in time, Phys. Rev. **138**, B979 (1965).

[45] A. Lichtenberg and M. Lieberman, *Regular and chaotic dynamics*, Applied mathematical sciences (Springer-Verlag, 1992).

[46] To break the reflection symmetry of the $\bar{\varepsilon}(z)$; we modify the additional modulation to $\lambda_b e^{(t-\gamma)^2/2\sigma^2}$ with $\gamma = 0.02$. If such a symmetry was present, the edge states would be superpositions of the localized wavepackets presented in Fig. 2(c).

[47] E. Lustig, Y. Sharabi, and M. Segev, Topological aspects of photonic time crystals, Optica **5**, 1390 (2018).

[48] K. Giergiel, A. Miroszewski, and K. Sacha, Time crystal platform: From quasicrystal structures in time to systems with exotic interactions, Phys. Rev. Lett. **120**, 140401 (2018).

[49] A. E. Kopaei, X. Tian, K. Giergiel, and K. Sacha, Topological molecules and topological localization of a rydberg electron on a classical orbit, Phys. Rev. A **106**, L031301 (2022).

[50] A. E. Kopaei, K. Giergiel, and K. Sacha, Topologically protected quantized changes of the distance between atoms (2024), arXiv:2406.19850 [cond-mat.quant-gas].

SUPPLEMENTAL MATERIAL: TOWARDS TIMETRONICS WITH PHOTONIC SYSTEMS

We begin with the original form of the Maxwell equations, which govern the behavior of the electric $\mathbf{E}$ and magnetic $\mathbf{H}$ fields in a medium:

$$\nabla \times \mathbf{E} = -\mu_0 \frac{\partial \mathbf{H}}{\partial t}, \quad \nabla \times \mathbf{H} = \varepsilon_0 \frac{\partial [\varepsilon(\mathbf{r},t)\mathbf{E}]}{\partial t}. \tag{6}$$

Here, μ_0 represents the vacuum permeability, and ε_0 is the vacuum permittivity and $\varepsilon(\mathbf{r},t)$ is the relative permittivity of a medium. To facilitate the analysis, we perform a re-scaling of the magnetic field, $\mathbf{H} \to \mathbf{H}\sqrt{\mu_0/\varepsilon_0}$. Moreover, for the ring-shaped resonator we consider in the main text, it is convenient to use $L/2\pi$ and $L/2\pi c$ as the units of length and time, respectively, where L is the circumference of the ring and $c = 1/\sqrt{\varepsilon_0\mu_0}$. This choice of units is particularly convenient for systems with a periodic geometry, as it naturally aligns with the symmetry of the problem. By scaling length by the factor $L/2\pi$, we effectively normalize the spatial dimension to the geometry of the ring, turning the circumference into 2π. Similarly, scaling time by $L/2\pi c$ normalizes temporal dynamics to the time it takes for light to travel around the ring. Under this transformation, we obtain

$$\nabla \times \mathbf{E} = -\frac{\partial \mathbf{H}}{\partial t}, \quad \nabla \times \mathbf{H} = \frac{\partial [\varepsilon(\mathbf{r},t)\mathbf{E}]}{\partial t}. \tag{7}$$

In a ring-shaped resonator with a square cross-section, as depicted in Fig. 1(a) in the main text, we analyze a scenario where the relative permittivity, $\varepsilon(\mathbf{r},t)$ is equaled to a constant value ε_r except within a localized segment in the resonator. In this segment, the permittivity is subject to periodic modulation over time. Specifically, the permittivity is modeled as

$$\varepsilon(\mathbf{r},t) = \varepsilon(z,t) = \varepsilon_r + h(z)f(t), \tag{8}$$

where z represents the position along the resonator circumference. The function $h(z)$ is spatially localized, effectively defining the region within the resonator where the permittivity varies in time. On the other hand, $f(t)$ is a periodic function with a period T, such that $f(t+T) = f(t)$, describing the time-dependent variation in the permittivity within the localized region, as illustrated in Fig. 1(b) in the main text.

We focus on the TE_{11} mode in the resonator. The appropriate ansatz which satisfies the metallic boundary conditions at $x = 0$ or a and $y = 0$ or a, where a is the length of each side of the cross-sectional area of the resonator [Fig. 1(a)], is given by

$$\begin{aligned}\mathbf{E} &= [\cos(k_\perp x)\sin(k_\perp y)\mathbf{e}_x - \sin(k_\perp x)\cos(k_\perp y)\mathbf{e}_y] \\ &\quad \times E(z,t) \\ \mathbf{H} &= [\sin(k_\perp x)\cos(k_\perp y)\mathbf{e}_x + \cos(k_\perp x)\sin(k_\perp y)\mathbf{e}_y] \\ &\quad \times H_t(z,t) + H(z,t)\cos(k_\perp x)\cos(k_\perp y)\mathbf{e}_z,\end{aligned} \tag{9}$$

where $E(z,t)$ and $H_t(z,t)$ represent the transverse components of the electric and magnetic fields, respectively, $H(z,t)$ is the longitudinal component of the magnetic field and $k_\perp = \pi/a$. It is worth noting that while a square cross-section is chosen here to simplify calculations, the main results will remain valid for a rectangular cross-sectional shape which is more common in photonic integrated circuits. Furthermore, for dielectric resonators the sinusoidal wave ansatz will change, but again the primary conclusions of the study will not be impacted.

The equation $\nabla \cdot \mathbf{H} = 0$ allows us to express $H_t(z,t)$ in terms of the longitudinal component,

$$H_t(z,t) = -\frac{1}{2k_\perp}\frac{\mathrm{d}H(z,t)}{\mathrm{d}z}. \tag{10}$$

Considering that $\varepsilon(z,t)$ is periodic in time such that $\varepsilon(z,t) = \varepsilon(z,t+T)$, the Floquet theorem [28, 44] implies that general solutions for the transverse electric and longitudinal magnetic fields can be expressed as superposition of $E(z,t) = \widetilde{E}(z,t)e^{i\omega t}$ and $H(z,t) = \widetilde{H}(z,t)e^{i\omega t}$ where $\widetilde{E}(z,t+T) = \widetilde{E}(z,t)$ and $\widetilde{H}(z,t+T) = \widetilde{H}(z,t)$ and the phase factors are determined by the quasi-frequencies ω, i.e. eigenvalues of the generalized eigenvalue problem,

$$\begin{bmatrix} -i\partial_t\varepsilon - i\varepsilon\partial_t & \frac{i}{2k_\perp}\partial_z^2 - ik_\perp \\ 2ik_\perp & -i\partial_t \end{bmatrix} \begin{bmatrix} \widetilde{E} \\ \widetilde{H} \end{bmatrix} = \omega \begin{bmatrix} \varepsilon & 0 \\ 0 & 1 \end{bmatrix} \begin{bmatrix} \widetilde{E} \\ \widetilde{H} \end{bmatrix}, \tag{11}$$

derived from the Maxwell equations (7), $\nabla \cdot \mathbf{H} = 0$ and $\nabla \cdot (\varepsilon(z,t)\mathbf{E}) = 0$. The permittivity $\varepsilon(z,t)$ is periodic in time and in the ring-shaped resonator, with the circumference of 2π in the units we use, it also fulfills $\varepsilon(z+2\pi,t) = \varepsilon(z,t)$. Thus, $\widetilde{E}(z,t)$ and $\widetilde{H}(z,t)$ fulfill periodic boundary conditions both in time and space and to solve the generalized eigenvalue problem (11), we can expand $\widetilde{E}(z,t)$ and $\widetilde{H}(z,t)$ in the basis $(2\pi T)^{-1/2}\sum_{n,m} e^{imz}e^{in\Omega t}$ where $\Omega = 2\pi/T$. The resulting matrix-form eigenvalue problem can be solved with standard routines.

In the main text we consider resonant driving of the system, i.e. the frequency Ω of the periodic modulation of the permittivity $\varepsilon(z,t)$ matches the free spectral range of the resonator. In other words we focus on electromagnetic waves with wave numbers close to k_0 for which the group velocity (calculated in the absence of the modulation) $\partial\omega/\partial k|_{k=k_0} = \Omega$ in the units we use. In such a case, we can simplify the description by deriving an effective counterpart of the Maxwell equations (11). First, let us switch to a reference frame moving with the resonant group velocity, $z' = z - \Omega t$, using the unitary transformation $U = e^{\Omega t\partial_z}$. Multiplying the rows of Eq. (11) by U and inserting the identity operator $1 = U^\dagger U$ leads, e.g. in the case of the second row, to

$$2ik_\perp U\widetilde{E}(z,t) - iU\partial_t[U^\dagger U\widetilde{H}(z,t)] = \omega U\widetilde{H}(z,t). \tag{12}$$

In the moving frame, we define the fields $\widetilde{E}'(z,t) = U\widetilde{E}(z,t)$ and $\widetilde{H}'(z,t) = U\widetilde{H}(z,t)$ and finally obtain the following eigenvalue equation,

$$\begin{bmatrix} -iU\partial_t(\varepsilon U^\dagger) - iU\varepsilon U^\dagger\partial_t & \frac{i}{2k_\perp}\partial_z^2 - ik_\perp \\ 2ik_\perp & -iU\partial_t U^\dagger - i\partial_t \end{bmatrix} \begin{bmatrix} \widetilde{E} \\ \widetilde{H} \end{bmatrix} = \omega \begin{bmatrix} U\varepsilon U^\dagger & 0 \\ 0 & 1 \end{bmatrix} \begin{bmatrix} \widetilde{E} \\ \widetilde{H} \end{bmatrix}, \tag{13}$$

where we have dropped the primes over the fields to simplify the notation.

If we consider the system with no modulation in time, $\varepsilon(z,t) = \varepsilon_r$, solutions of Eq. (13) can be chosen in the form of $\widetilde{E}(z,t) = E_0 e^{ikz}$ and $\widetilde{H}(z,t) = H_0 e^{ikz}$ with constant E_0 and H_0 and the corresponding eigenvalue,

$$\omega(k) = \sqrt{\frac{1}{\varepsilon_r}(k^2 + 2k_\perp^2)} - \Omega k. \tag{14}$$

The fields have to fulfill the periodic boundary conditions in the ring-shaped resonator, hence, the dispersion relation (14) actually consists of points corresponding to integer values of the wave number k.

The dispersion relation (14) possesses a minimum at

$$k_0 = \frac{\sqrt{2\varepsilon_r}\Omega k_\perp}{\sqrt{1-\varepsilon_r\Omega^2}}, \tag{15}$$

see Fig. 1 in the main text. Around this minimum,

$$\omega(k) \approx \omega(k_0) + \frac{\varepsilon_r\Omega^3 k_\perp^3}{k_0^3}(k-k_0)^2, \tag{16}$$

and the group velocity is very small. Consequently a wave-packet being superposition of waves with the wave numbers $k \approx k_0$ propagates very slowly. Thus, when the modulation of the permittivity is on and it is weak, to describe the system we may average the exact Maxwell equations (13) over time (rotating wave approximation) and obtain effective time-independent Maxwell equations,

$$\begin{bmatrix} i\Omega\partial_z\bar{\varepsilon} + i\Omega\bar{\varepsilon}\partial_z & \frac{i}{2k_\perp}\partial_z^2 - ik_\perp \\ 2ik_\perp & i\Omega\partial_z \end{bmatrix} \begin{bmatrix} \widetilde{E} \\ \widetilde{H} \end{bmatrix} = \omega \begin{bmatrix} \bar{\varepsilon} & 0 \\ 0 & 1 \end{bmatrix} \begin{bmatrix} \widetilde{E} \\ \widetilde{H} \end{bmatrix}, \tag{17}$$

where the averaged permittivity

$$\bar{\varepsilon}(z) = \varepsilon_r + \frac{1}{T}\int_0^T \mathrm{d}t\; h(z+\Omega t) f(t). \tag{18}$$

The comparison between the results obtained from the effective time-independent equations (17) and the exact Maxwell equations (13) for two distinct cases of the permittivity function $\varepsilon(z,t)$ is illustrated in Figs. 2-3 in the main text. These figures clearly demonstrate that the effective approach captures the essential physics of the system while significantly reducing computational complexity and facilitating deeper intuitive insights.